Adaptive Bayesian Sparse Polynomial Chaos Expansion for Voltage Balance of an Isolated Microgrid at Peak Load

Rashmi Agarwal [1], Sunil Kumar [2*], and Harivardhagini Subhadra [3]

[1] Department of Electrical Engineering, J.C. Bose University of Science and Technology YMCA, Faridabad, India

[2*] Department of Electrical Engineering, Jamia Millia Islamia, New Delhi, India

[3] Department of Electrical Engineering, CVR College of Engineering, Telangana, India

rashmiagarwal404@gmail.com, *skk7503@gmail.com, harivardhagini@cvr.ac.in

ABSTRACT

Microgrids (MGs) are essential for ensuring a reliable and efficient power supply, particularly in isolated or islanded regions. One of the significant challenges faced is maintaining voltage balance during peak load periods, which is complicated by uncertainties in renewable energy availability, demand response, and system constraints. This paper introduces an Adaptive Bayesian Sparse Polynomial Chaos Expansion (BSPCE) framework designed to tackle these challenges effectively. Unlike traditional BSPCE methods that utilize fixed sampling strategies, our adaptive approach dynamically modifies sampling locations in response to approximation errors or model sensitivities. This allows for a more efficient allocation of computational resources, enhancing approximation accuracy in areas of high uncertainty. The framework systematically quantifies uncertainties related to maximum loadability and operational constraints while also accounting for the impacts of battery energy storage systems, electric vehicles, and demand response mechanisms. By applying this methodology to the IEEE-15 bus system, we provide a comprehensive assessment of voltage balance in isolated microgrids during peak load conditions. The proposed method is capable of dealing with a large number of correlated inputs and following unrelated distributions. The simulation modeling is performed on the MATLAB platform. The numerical results from the IEEE 15 test feeders confirm that the approach is accurate and efficient at the same time.

Index-words: Microgrids, Peak load, Renewable energy source, Electric vehicle system, IEEE 15 bus.

Nomenclature	
P_{di}	Active power of dispatchable sources
Q_{di}	Reactive power of dispatchable sources
$Q_{di,ub}$	The upper bound of reactive power of dispatchable sources
$P_{di,ub}$	The upper bound of the real power of dispatchable sources
m_{pi}	Droop gains of real power
n_{qi}	Droop gains of reactive power
V_0	Nominal voltage
V	System voltage
f_0	Nominal frequency
f	System frequency
$P_{dch,t}^{MG}$	Discharging power in kW of MG
$X_{t,ch}^{MG}$	Status of charging
$X_{t,dch}^{MG}$	Status of discharging
SoC_{min}^{MG}	Minimum SoC of MG
SoC_{max}^{MG}	Maximum SoC of MG
η_{ch}^{BESS}	Charging efficiency of BESS
η_{dch}^{BESS}	Discharging efficiency of BESS
$P_{dch,t}^{BESS}$	Discharging power in kW
$P_{ch,t}^{BESS}$	Charging power in kW
OC_{G1}^{t}	Operational costs of the dispatchable generator 1
q	Shape parameter
c	Scale value
v	Random variable
μ	Mean
γ	Standard deviation
V_i^{lb}, V_i^{ub}	Lower and upper bounds on voltage at 'i^{th}' bus
P_{gi}^{lb}, P_{gi}^{ub}	Lower and upper bounds on active power generation at 'i^{th}' bus
Q_{gi}^{lb}, Q_{gi}^{ub}	Lower and upper bounds on reactive power generation at 'i^{th}' bus
$P_{dg,i}^{t}$	Power generation by diesel generator at 'i^{th}' bus
$P_{RES,i}^{t}$	Power generation by RESs at 'i^{th}' bus
P_{ij}^{lb}, P_{ij}^{ub}	Lower and upper bounds on active power transmission between 'i^{th}' bus and 'j^{th}' bus
$P_{BESS,i}^{t}$	Power available at time 't' across BESS

I.   INTRODUCTION

A.   Motivation

Today, the country has an overdemand for electricity due to its population. This over stressed existing power systems [1]. Such generators are dispatchable, but some of these drawbacks do not make these sources economical, environment unfriendly, and unsustainable in nature. As fundamental components of modern power systems, microgrids are regarded as an effective means to improve reliability, flexibility, and resilience in regions subject to disturbances of power. The operations can be in islanded or grid-connected mode. The microgrid will be required to behave according to voltage and frequency rules prescribed by the utility grid when modeled as an infinite bus and connected to the grid [2]. In such a case, distribution generation units control the voltage and frequency in accordance with their droop characteristics [3]. The implementation of this system provides advantages in terms of grid resilience and the reliability of power systems during periods of disruption.

The operation of MG uses largely renewable energy sources (RES) such as wind turbines (WT) and photovoltaic (PV) systems that usually operate in maximum power point tracking (MPPT) mode [4] [5] constrained for grid connected cases to optimize energy management. In the determined state of charge (SoC) [6], surplus energy is supplied to the main grid or stored in the battery energy storage systems (BESS). The mode of operation for the RES is influenced by the level of SoC in the system. Any additional load is covered by power from the BESS. Whereas the voltage controls PV output and wind turbines base their output power on pitch control, RES output is reduced in an off-MPPT system. RESs rely on MPPT, but the BESS responds to the energy gaps between what is being produced and used [7]. The direction, turbulence, and variation of wind speed play a role in deciding how wind power is generated in microgrids. Additionally, load demand fluctuates due to meteorological conditions, economic activity, and consumer behavior. However, these uncertainties can lead to voltage balance disturbance and cause system instability in the case of peak load, especially [8]. This paper presents a BSPCE framework to address these challenges with the aim of improving isolated microgrid voltage balance assessment at peak load. By adopting a dynamic sampling strategy in modeling sensitivity and uncertainty, problems with variation in model sensitivities are integrated into the proposed approach, whereby both uncertainties quantification and computational resource allocation are quantified systemically. This adaptive method provides us with a useful tool for analyzing and reducing the uncertainties in microgrid operation and improving microgrid's resilience and reliability.

A variety of surrogate modeling and sensitivity analysis methods are used to manage uncertainty in power system analysis in this research. The Sparse Polynomial Chaos Explosion (SPCE) method [9] is used to create efficient surrogate models at a lower computational cost while maintaining accuracy. This paper introduces a BSPCE that builds upon SPCE by incorporating Bayesian model selection to select the most relevant polynomial basis functions. Global Sensitivity Analysis (GSA) [10] is a framework for identifying the input uncertainties that impact output variability. It is essential to note that GSA and BSPCE are distinct concepts, although they are closely related in the modeling process, with BSPCE being an extension of the former.

B.   Research Gap

However, the operation of microgrids in islanded configuration requires advanced methodologies; here, uncertainty exists in renewable energy generation, load, and system constraints. There have been several studies in the domain of optimization and control strategies to enhance the stability, loadability, and resilience of islanded microgrids (IMGs) [11], [12]. The probabilistic approach [13] is used to optimize droop settings in diesel generator (DG)-based distribution networks. This method improves IMG performance without a microgrid central controller (MGCC) by extending the loading margin and staying within system constraints. Later [14] was extended to use GSA for evaluating the loadability of the IMG under renewable energy variability using probabilistic nonlinear optimization, together with conditional probability and Copula functions. The insights from this approach were in terms of how the DG droop characteristics and network parameters influence IMG performance. The use of surrogate models for evaluating the load margin has also played a crucial role in its development. The concept of a reduced islanded microgrid network was introduced in [15], which encompassed power flow methods and a general distributed sensitivity index for multi-bus microgrids. A strategy for dividing active distribution networks into self-

sustaining isolated areas was put forward in [16], which entailed creating new constraints for load capacities that preserved the radial structure of the generated isolated networks. Advanced sensitivity analysis techniques [17] have further contributed to understanding IMG loadability. The Borgonovo method, a density-based GSA approach [18], is used to quantify the influence of uncertainties on maximum IMG loadability. The computational efficiency was improved by combining Polynomial Chaos Expansion (PCE) with Kriging models, known as PCE-Kriging, to provide surrogate models for sensitivity analysis [19]. Monte Carlo Simulations (MCS) [20] are computationally expensive and possess high accuracy. Point estimation [21] and cumulant-based methods [22] are efficient, but they can be challenging to apply when the inputs are conditioned or non-Gaussian in nature. Developing advanced models such as kriging or neural networks requires a large database and a more extensive training process.

Much research has been conducted on how the grid handles stable power loss and isolation. The risks of voltage instability in different microgrid configurations (dc-ac and ac-dc) were evaluated in [23], emphasizing the significance of droop parameters and DGs in preserving voltage stability. The study also revealed that saddle-node bifurcation (SNB) is a primary cause of voltage instability in DC microgrids. A control method [24] has been proposed to address the problems posed by imbalanced and harmonically distorted loads on the stability of microgrids. Microgrid research has extensively focused on resolving complex Optimal Power Flow (OPF) problems. A comprehensive study in [25] was performed on droop-controlled IMGs, focusing on three challenges: a bi-objective OPF for minimizing cost and ensuring loadability, evaluating maximum loadability, and optimizing system loadability. The main concern with these strategies is ensuring loadability, which serves as a leading performance indicator in IMG planning.

C.   Contribution

Recent studies [26] have shown that adaptive sampling strategies for Bayesian Sparse Polynomial Chaos Expansion (BSPCE) enable dynamic adjustments to be made in sampling locations based on approximation errors or model sensitivity. This research presents a new Adaptive Bayesian Sparse Polynomial Chaos Expansion (BSPCE) method designed for handling voltage balancing issues in isolated microgrids when peak load occurs. A new Adaptive Bayesian Sparse Polynomial Chaos Expansion (BSPCE) framework was created to solve problems related to voltage imbalance in isolated microgrids during peak load periods. A new approach was developed that takes into account adaptive sampling methods for BSPCE, allowing for the dynamic adjustment of sampling points based on the current approximation error or the model's sensitivity to input parameters. The study further investigates the effect of demand response on the voltage profile at bus 9, offering valuable insights into the localized effects of demand-side management strategies on distribution system stability and reliability.

The paper provides a significant contribution to the understanding of electric vehicle integration by examining its impact on the voltage profile at bus 14. The study examines the influence of battery energy storage systems on the voltage profile at bus 8.

II.   MODELING OF PROPOSED SYSTEM

This section outlines models for distributed generation units and loads and then proceeds with the development of probability models for input parameters. A stochastic optimization framework was subsequently developed to assess the maximum loadability of the isolated microgrid (IMG). Probability distribution selection depends on the way renewable energy behaves and on load patterns, and often, the Normal distribution is a suitable approximation, although there may be occasional inconsistencies. Since uncertainties in PV, wind, and load demand all have an impact on each other, they significantly affect the stability and performance of a microgrid. As power generation grows or drops, it can disturb the balancing act between supply and demand, so grid reliability depends on energy storage and generation being regulated. The layout of power and information flow within microgrid components is depicted in Fig. 1.
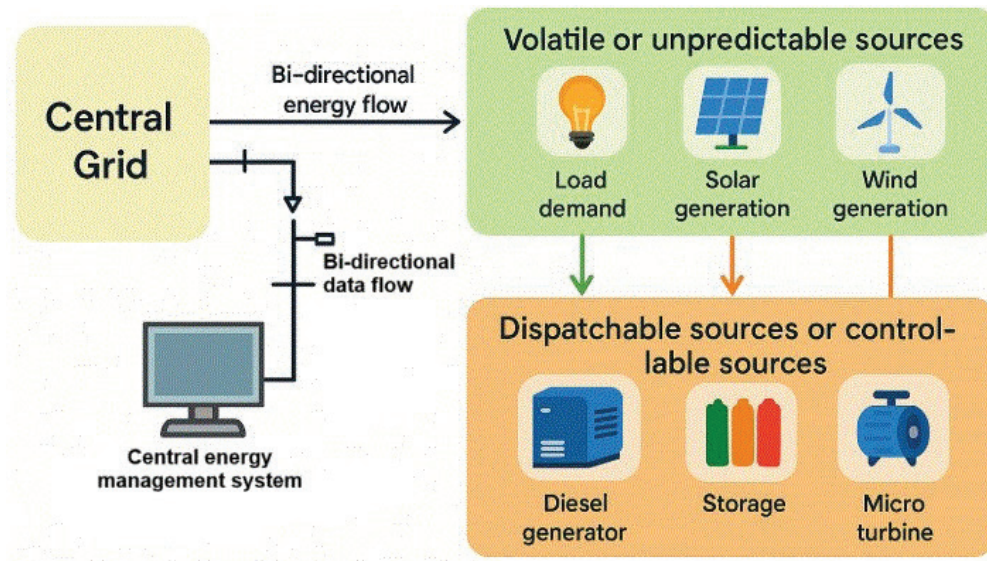
Fig. 1. Grid interfaced MG for power flow and information

A.   Load Forecasting Modeling

Load demand for the MG system fluctuates throughout the day due to factors such as weather, economic activity, and consumer behavior patterns. Load demand can vary stochastically or predictably due to numerous factors, including seasonal fluctuations, weekday patterns, and daily time slots. The probability distribution function (PDF) of load demand follows a normal distribution characterized by the following specifications [27]:

$$f(L) = \frac{1}{\sigma\sqrt{2\pi}} e^{-\frac{(L-\mu)^2}{2\sigma^2}} \tag{1}$$

Where μ and σ represent the mean load and standard deviation value for electrical load, the electrical load is denoted by L. Normal distribution remains a practical approach for estimating data in bulk collections, even if some data may be heavy-tailed or irregularly skewed.

B.   Wind Turbine Modeling

Wind turbines convert the kinetic energy of wind into electrical power, and their performance is modeled using the Weibull distribution, which effectively represents the variability and intermittency of wind resources. The PDF of wind speed is given as [28]:

$$PDF(v) = \frac{q}{c}\left(\frac{v}{c}\right)^{q-1} exp\left(-\left(\frac{v}{c}\right)^q\right) \tag{2}$$

$$q = \left(\frac{\delta}{\mu}\right)^{-1.086} \tag{3}$$

$$c = \frac{\mu}{\gamma\left(1+\frac{1}{h}\right)} \tag{4}$$

The parameter q signifies the shape, with c representing the scale value and v denoting the random variable. The Weibull distribution's shape parameter affects its skewness and kurtosis, which in turn influence the distribution's overall characteristics. This makes it well-suited to capturing the variability and intermittency of wind resources. When q>1, the distribution indicates an increasing frequency of higher wind speeds, making it ideal for regions with consistent high-speed winds. Conversely, for 0<q<1, the distribution reflects a decrease in wind speed frequency as the speed increases.

C.   Solar Energy Generation Modeling

The implementation of PV energy production depends on multiple influences that include changing weather patterns as well as cloud patterns and amount of solar irradiance along with daily time periods. PV output random fluctuations undergo modeling by means of Beta distribution because this distribution works within the [0,1] range which matches PV operational ranges [29].

$$f(x) = \frac{x^{\alpha-1}(1-x)^{\beta-1}}{B(\alpha,\beta)} \tag{5}$$

$$B(\alpha,\beta) = \frac{\gamma(\alpha)\gamma(\beta)}{\gamma(\alpha+\beta)} \tag{6}$$

D. Droop-Controlled Power Sources

A P-f/Q-V droop control strategy maintains system stability for the dispatchable sources. This control is characterized by linear relationships between active/reactive power and frequency/voltage deviations [30].

$$P_{di}m_{pi} = f_0 - f \tag{7}$$

$$Q_{di}n_{qi} = V_0 - V \tag{8}$$

$$P_{di,ub} - P_{di} \geq 0 \tag{9}$$

$$f_0 - f - P_{di}m_{pi} \geq 0 \tag{10}$$

$$(P_{di,ub} - P_{di})(f_0 - f - P_{di}m_{pi}) = 0 \tag{11}$$

$$Q_{di,ub} - Q_{di} \geq 0 \tag{12}$$

$$V_0 - V - Q_{di}n_{qi} \geq 0 \tag{13}$$

$$(Q_{di,ub} - Q_{di})(V_0 - V - Q_{di}n_{qi}) = 0 \tag{14}$$

The active and reactive powers of dispatchable sources are described using P_{di} and Q_{di}, while the system works with f_0 and V_0 as the nominal frequency and voltage values. Real and reactive power droop coefficients can be found in the expressions through m_{pi} and n_{qi}. The current frequency and voltage levels of the system are represented by f and V, respectively. Additionally, $P_{di,ub}$, $Q_{di,and\ ub}$ signify the maximum values for the active and reactive power output of dispatchable sources.

E. Energy Storage System (ESS)

Renewable energy generation variability is largely dependent on the functionality of BESS. The operational strategy of the EVS is defined based on its charging and discharging states [31], [32]:

$$SoC_{t+1}^{MG} = SoC_t^{MG} + \Delta T \left(\eta_{ch}^{BESS} P_{ch,t}^{BESS} - \frac{P_{dch,t}^{BESS}}{\eta_{dch}^{ESS}} \right) \tag{15}$$

$$SoC_{min}^{MG} \leq SoC_t^{MG} \leq SoC_{max}^{MG} \tag{16}$$

$$0 \leq P_{ch,t}^{MG} \leq X_{t,ch}^{MG} P_{ch}^{MG} \tag{17}$$

$$0 \leq P_{dch,t}^{MG} \leq X_{t.dch}^{MG} P_{dch}^{MG} \tag{18}$$

$$X_{t,ch}^{MG} + X_{t.dch}^{MG} \leq 1 \tag{19}$$

$X_{t,ch}^{MG}$, $X_{t,dch}^{MG}$ represents the charging and discharging status, respectively. The symbols SoC_{min}^{MG} and SoC_{max}^{MG} represent the lowest and highest state of charge (SoC) levels of the IMG. The notations η_{ch}^{EVS} and η_{dch}^{EVS} denote the efficiency of BESS when charging and discharging. Furthermore, $P_{ch,t}^{EVS}$, $P_{dch,t}^{EVS}$ and signify the capacity of the BESS to charge and discharge power.

F. Loadability Assessment Modelling

The microgrid load ability analysis takes place through a stochastic optimization process with numerous constraints [33]:

$$V_i^{lb} \leq V_i \leq V_i^{ub} \tag{20}$$

$$P_{gi}^{lb} \leq P_{gi} \leq P_{gi}^{ub} \tag{21}$$

$$Q_{gi}^{lb} \leq Q_{gi} \leq Q_{gi}^{ub} \tag{22}$$

$$P_{ij}^{lb} \leq P_{ij} \leq P_{ij}^{ub} \tag{23}$$

$$\sum_{t=1}^{24} \sum_{i=1}^{33} P_{dg,i}^t - P_{l,i}^t + P_{RES,i}^t \pm P_{ESS,i}^t = 0 \tag{24}$$

The voltage values at bus station i^{th} must exist between V_i^{lb} and V_i^{ub} to satisfy the established voltage restriction levels. The power generation limits at the ith bus can be found through P_{gi}^{lb} and P_{gi}^{ub}. Reactive power generation at ith bus comes with constraints defined by Q_{gi}^{lb} and Q_{gi}^{ub}. At any given time t, the power output level of the diesel generator at the ith bus is designated as $P_{dg,i}^t$.

The complete modeling system represents all elements within renewable power generation as well as load patterns and storage devices in an isolated microgrid to assess voltage stability and peak performance capabilities.

III. PROPOSED TECHNIQUE

The proposed technique, illustrated in Fig. 2, improves the accuracy and computational efficiency of modeling isolated microgrid peak load voltage regulation with a Sparse Polynomial Chaos Expansion method. SPCE alleviates the PCE computational load by choosing only a subset of the expansion terms. During the selection process, the size of the coefficients, their role in the problem, and their statistical significance were all considered. A few common techniques - least-angle regression, the least absolute shrinkage and selection operator (LASSO) method, and sequential thresholding are applied to find the PC coefficient. Typically, this method involves addressing a linear regression problem, where the model's output serves as the response variable, and the chosen polynomial terms

are the input parameters. To take advantage of Bayesian methodology and prior experience, BSPCE is used. A Sobol decomposition method was used to find out which factors from the microgrid inputs had the greatest impact on its loadability.

A. SPCE Method

Let A be a finite subset of $\mathbb{N}^n$, with constrained Polynomial Chaos Expansion (PCE):

$$\mathcal{M}_{X(a)} = \sum_{\alpha \in X} d_\alpha \mu_\alpha(a) \qquad (25)$$

The common truncation scheme is denoted $X = X^{p,n}$, which means it represents the full PCE. However, because the cardinality of this set can be very high, which can cause tough computations, it matters to discover truncation sets X that consist of less data. If the following criterion is met, the PCE can be called a sparse truncated PCE:

$$IS = \frac{card(X)}{card(X^{p,n})} \ll 1, \quad p = \max_{\alpha \in X}(|\alpha|) \qquad (26)$$

For this study, a new algorithm relying on Bayesian model selection is suggested to construct sparse PCEs.

B. PCE-based Global Sensitivity Analysis

Implementation of the PCE model enables the rapid assessment of global sensitivity using Sobol indices. Let us study the PCE in Equation (25). The definition of a subset of multi-dimensional indices $\zeta_{i_1 \ldots \ldots i_s}$ for X is defined as:

$$\zeta_{i_1 \ldots \ldots i_s} = \left\{ \alpha \epsilon X : \begin{matrix} \alpha_k > 0 & k \in (i_1 \ldots \ldots i_s) \\ \alpha_k = 0 & k \in (i_1 \ldots \ldots i_s) \end{matrix} \quad for \ \forall k = 1, \ldots ., n \right\} \quad (27)$$

With this notation, the sparse PCE becomes written as a Sobol's decomposition:

$$\mathcal{M}_X = d_0 + \sum_{i=1}^n \sum_{\alpha \epsilon \zeta_{i_1}} d_\alpha \mu_\alpha(a_{i_1}) + \sum_{i_2 > i_1}^n \sum_{\alpha \epsilon \zeta_{i_1 i_2}} d_\alpha \mu_\alpha(a_{i_1}, a_{i_2}) + \sum_{i_s > \cdots > i_1}^n \sum_{\alpha \epsilon \zeta_{i_1, \ldots, i_s}} d_\alpha \mu_\alpha(a_{i_1} \ldots, a_{i_s}) + \cdots + \sum_{\alpha \epsilon \zeta_{1, \ldots n}}^n d_\alpha \mu_\alpha(x) \qquad (28)$$

Each term $\mathcal{M}_{i_1 \ldots i_s}(a_{i_1, \ldots,} a_{i_s})$ can be identified as:

$$\mathcal{M}_{i_1 \ldots i_s}(a_{i_1, \ldots,} a_{i_s}) = \sum_{\alpha \epsilon \zeta_{i_1, \ldots, i_s}} d_\alpha \mu_\alpha(a_{i_1} \ldots, a_{i_s}) \quad (29)$$

Total and partial variances:

$$D_X = \sum_{\alpha \epsilon X \backslash \{0\}} d_\alpha^2, \quad D^X_{i_1 \ldots i_s} = \sum_{\alpha \epsilon \zeta_{i_1, \ldots, i_s}} d_\alpha^2 \qquad (30)$$

Partial sensitivity indices:

$$S^X_{i_1 \ldots i_s} = \frac{D^X_{i_1 \ldots i_s}}{D^X} \qquad (31)$$

Total sensitivity index:

$$S^{T,X}_i = \sum_{\alpha : \alpha_i > 0} S^X_\alpha \qquad (32)$$

C. Bayesian Ensemble Modeling Framework

Consider a set of N_m plausible sparse PCE models $\mathcal{M}_{Xk}$ being available.

$$\mathcal{M}_{Xk} = \sum_{\alpha \in Xk} d_\alpha \mu_a, \quad k = 1, \ldots., N_m \qquad (33)$$

The vector form of the above equation is written as $\mathcal{M}_{Xk} = d_k \mu_k$. This research aims to choose the best sparse PCE, given input-output data A and B, using Bayesian Model Averaging. The posterior probabilities function through Bayes 'theorem:

$$P\left(\frac{\mathcal{M}_{Xk}}{y}\right) = \frac{P\left(y / \mathcal{M}_{Xk}\right) P(\mathcal{M}_{Xk})}{\sum_{i=1}^{N_m} P\left(y / \mathcal{M}_{X_i}\right) P(\mathcal{M}_{X_i})} \qquad (34)$$

The model evidence is estimated via:

$$P\left(\frac{y}{\mathcal{M}_{Xk}}\right) = \int P\left(\frac{y}{\mathcal{M}_{Xk}}, d_k\right) P\left(\frac{d_k}{\mathcal{M}_{Xk}}\right) dd_k \qquad (35)$$

Laplace approximation gives:

$$P\left(\frac{y}{\mathcal{M}_{Xk}}\right) \simeq P\left(\frac{y}{\mathcal{M}_{Xk}}, \widetilde{d_k}\right) P\left(\frac{\widetilde{d_k}}{\mathcal{M}_{Xk}}\right) (2\pi)^{P_k/2} \left|\widetilde{\Sigma}\right|^{-1/2} \qquad (36)$$

Kashyap information criterion (KIC) is obtained by considering that the posterior distribution is very similar to a Gaussian distribution and is close to its Maximum A Posteriori (MAP) value.

$$KIC_k = -2 \ln P\left(\frac{y}{\mathcal{M}_{Xk}}, \widetilde{d_k}\right) - 2 \ln P\left(\frac{\widetilde{d_k}}{\mathcal{M}_{Xk}}\right) - P_k \ln(2\pi) - \ln|C_{\tilde{d}\tilde{d}}| \quad (37)$$

D. Adaptive BSPCE Algorithm

Assume that we have A = {A (1), . . ., A⁽ᴺ⁾} with N apprehensions, based on Monte Carlo Simulations (MCS). The responses from the model are gathered and organized into the vector B = {B⁽¹⁾, . . . , B⁽ᴺ⁾}ᵀ after running the model at different time intervals. During the initialization stage, the data (A, B) are transformed into homogeneous vectors (a, b) as part of employing the Bayesian model averaging (BMA) framework, making it feasible to devise an algorithm for selecting the most suitable sparse PCE model from the dataset. Next, the principal degree and interaction order of the PCE are determined based on the characteristics of the model's response of interest. Following this, a subsequent subset is generated:

Step-1 Initialization data: Standardized vectors (x, y) are made from the original data (X, Y). After that, the distinguishing characteristics of the PCE are chosen by defining both p and q; you should use (p = 2, q = 1) or (p = 4, q = 2) depending on the features of the response from your model. After that, a special subset like this is chosen:

$$X^{p,q} = \{\alpha \in \mathbb{N}^n : p_\alpha \le p; q_\alpha \le q\}/\{0\} \qquad (38)$$

Step-2 Correlation-based ranking: Ranking by correlation coefficient involves defining P as the cardinality of $X^{p,q}$ and elucidating the polynomial basis μ = (μ$_1$, μ$_2$,..., μ$_p$) associated with $X^{p,q}$. Subsequently, calculate the Pearson correlation coefficient 's_j' between each polynomial term $μ_j(a)$ ∀ j = 1, . . ., P and the model response vector 'b' in the following manner:

$$s_j = \frac{Cov[b, μ_j(a)]}{\sqrt{V[b] * V[μ_j(a)]}} \qquad (39)$$

The array $(s_1^2, s_2^2, \ldots, s_P^2)$ is sorted in descending order, and the corresponding polynomial basis functions are rearranged into a new vector $μ = μ_1, μ_2, \ldots, μ_P$ ensuring that $s_j^2 \ge s_{j+1}^2$.

Step-3 Partial correlation-driven prioritization: Ranking through the partial correlation coefficient involves calculating the partial correlation coefficient $\hat{s}_{j|1,\ldots,j-1}$ or each basis function $\hat{μ}_j(a)$ and b for j = 1, . . ., P using the following equation:

$$\hat{s}_{j|1,\ldots,j-1} = \frac{Cov[b, \hat{μ}_j(a), |\hat{μ}_1(a), \ldots, \hat{μ}_{j-1}(a)]}{\sqrt{V[b|\hat{μ}_1(a), \ldots, \hat{μ}_{j-1}(a)] \, V[\hat{μ}_j(a)|\hat{μ}_1(a), \ldots, \hat{μ}_{j-1}(a)]}} \qquad (40)$$

The conditional covariance operator is represented by COV [·|·], and the conditional variance operator by V [·|·]. The array ($\hat{s}_1^2, \hat{s}_{2|1}^2, \hat{s}_{3|1,2}^2, \ldots, \widehat{s}_{P|1..P-1}^2$) is then sorted in descending order, similar to Step 2. This sorting facilitates the update of the vector $\hat{μ} = (\hat{μ}_1, \hat{μ}_2, \ldots, \hat{μ}_P)$ of Polynomial Chaos (PC) basis elements such that $\hat{s}_{j|1,\ldots j-1}^2 \ge \hat{s}_{j+1|1,\ldots j}^2$.

Step-4 Formulation of the selected sparse PCE: The identification of the current sparse PCE is carried out by describing a sparse PCE model $\mathcal{M}_{X_k}$ using the polynomial $μ_k$ = ($μ_X, μ_k$). Utilizing the BMA method, we assess the current sparse PCE model, M_{X_k}. This involves evaluating the MAP estimates $\hat{d}_k$ and $C_{\hat{d}\hat{d}}$, alongside determining the KIC_k assigned to the current model. M_{X_k}. If $KIC_k \le KIC_{k-1}$, set μ$_X$= μ$_K$ and $d_X = \tilde{d}_k$, otherwise set $KIC_k = KIC_{k-1}$. Next, increment k by one and iterate through this process until k equals P.

Step-5 Enhancing the approximation space $X^{p,q}$ **:** To enrich $X^{p,q}$, express $\mathcal{M}_X = d_X μ_X$ for the identified SPCE, where the elements correspond to the subset X. If the subset X contains (i) elements of degree p−1 or p, then $p = p + 2$ or (ii) elements with interaction level q, then increment in $q = q + 1$

and restart the second step by setting $X^{p,q}$ = X, and enrich the subset by adding elements of degree p−1 and p, as well as elements with interaction level q. If neither condition is satisfied, terminate the computation. The algorithm starts by considering all the PC basis elements of low degree (typically p = 2) and low level of interactions (q = 1). This ensures that the initial number of elements to be analyzed with the KIC is small. For issues with high dimensions (n>10), considering all possible interaction levels (q+1) in Step 5 can result in a large array of terms in $X^{p,q}$. Therefore, only the changes related to the relevant inputs of the current iteration are considered during this phase. While this proposed enhancement strategy helps reduce computational costs, it frequently results in identifying a sparse PCE that performs sub-optimally.
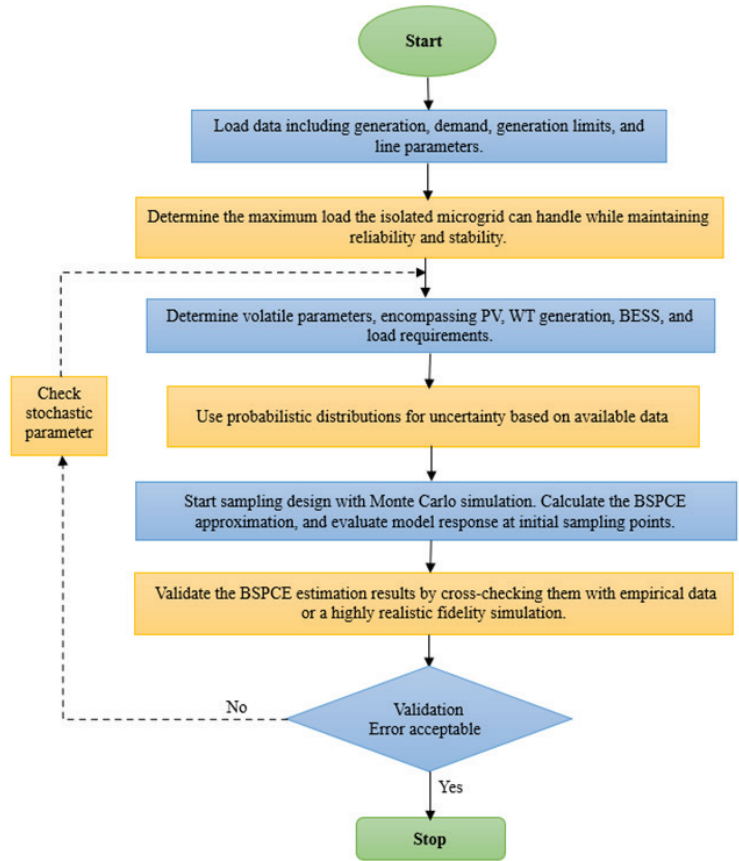

Fig. 2. Proposed methodology

This study found that setting $σ_X^2 < 0.05$ in an SPCE is beneficial. If this happens, it is better to identify PCE again by increasing the initial values of p and q. If the results above are not satisfactory, then the model response vector B can be updated and the experimental design A fixed before retrying the optimal SPCE identification.

IV. RESULTS AND DISCUSSIONS

A modified IEEE-15 bus test system was considered for an isolated microgrid operating at maximum demand and was simulated on MATLAB, as depicted in Fig. 3. Three distributed generators were installed at buses 4, 8, and 12. The first DG has an active power capacity of 3 MVA and a reactive power capacity of 1.5 MVA, while the second has an active power capacity of 0.5 MVA and a reactive power capacity of 1 MVA. The third DG has an active power capacity of 1.5 MVA and a reactive power capacity of 1 MVA. The nominal voltages are 1.0009, 1.0008, and 1.0009, while the nominal frequencies are 1016, 1.016, and 1.040. Stochastic photovoltaic generation was initially implemented at buses 8 and 10, featuring a 0.75 MVA capacity and a 0.9 lagging power factor. Additionally, wind turbines (WT) were installed on buses 13 and 15, both having the same specifications and operating power factor.
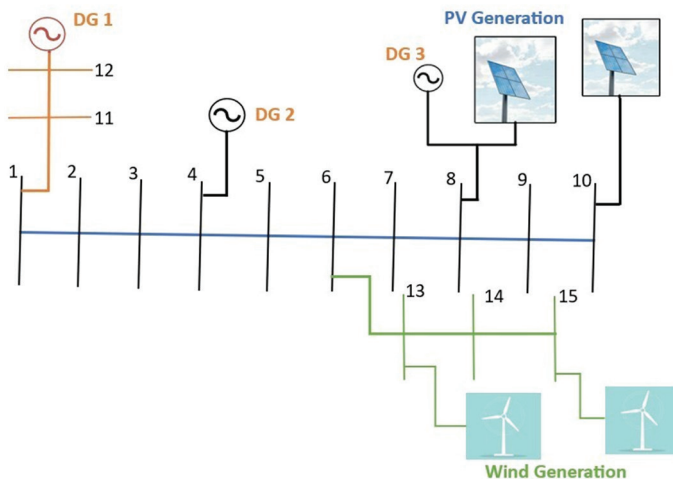

Fig. 3. Modifies IEEE-15 bus test system under consideration

The coefficients for significant terms were calculated by applying regression techniques after their identification. So, in SPCE, the solution is often found with linear regression, where the model outputs the response and takes input from chosen polynomial terms. It is built on the foundation of SPCE while using Bayesian inference. The coefficients' posterior distribution was approximated in this work using Bayesian regression on the data. In this part, we explain how different random variables can affect the IMG load margin according to the proposed method. Each model's results are compared with those of GSA-PCE, GSA-SPCE and GSABSPCE. All methods gave similar GSs when the sample was large. Fig. 4 shows the index number for input variables assuming deterministic renewable energy sources, while Fig. 5 illustrates the index of input

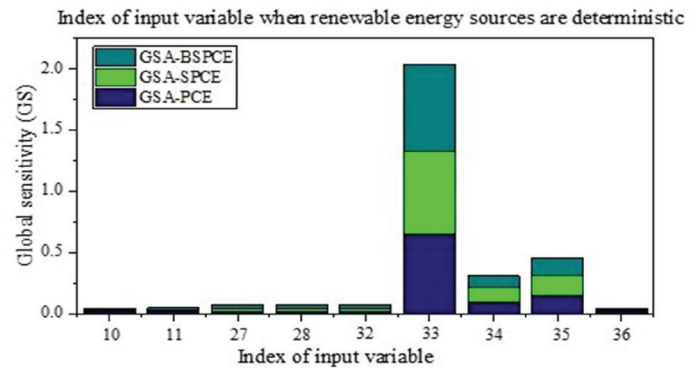variables under conditions of volatile or stochastic RESs.

Fig. 4. Deterministic RESs typically rely on a fixed index of input variables

The bus with RESs in it, as illustrated in Fig. 5, exhibits heightened sensitivity, primarily due to the volatile characteristics of RESs. The GS values of the WT output power for buses 13 and 15 are shown in Fig. 6. GSA-PCE is less precise than GSA-SPCE, as it requires several samples to establish the surrogate model coefficient. The cumulative probability density functions (CDF) graph depicted in Fig.7 displays the distribution of the load margin under different operating conditions, acting as a primary result of the BSPCE model for assessing voltage stability in isolated microgrids during peak loads.
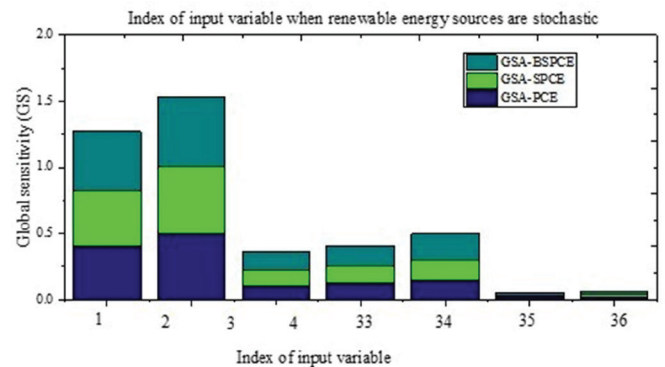

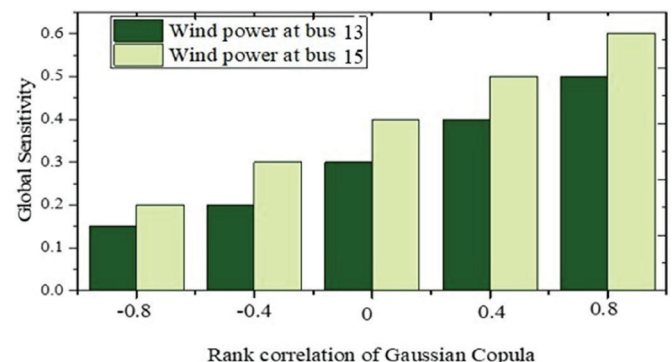Fig. 5. Stochastic RES input variable index
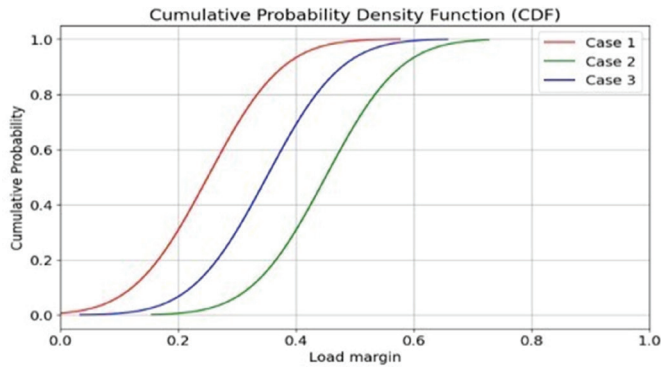

Fig. 6. Global sensitivity of wind power

Fig. 7. Cumulative probability density function for 3 cases

This emphasizes the effects of renewable energy variability and uncertainty in demand, with Case 3 showcasing enhanced resilience in voltage. This shows the accuracy of the model and gives useful information when planning for a microgrid by estimating the risk of voltage collapse. Fig. 8 illustrates the load demand for a 24-hour scheduling interval, accompanied by the available generation and the energy exchange with the BESS. In the context of voltage balance within an IMG system utilizing uncertain renewable energy sources, stochastic optimization surpasses robust optimization in terms of precision.
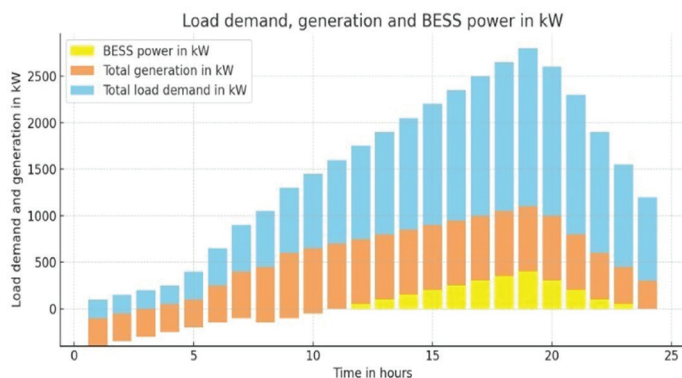

Fig. 8. Load profile, generation, and battery exchange

The research considered stochastic optimization for managing voltage and energy in a microgrid, encompassing solar, wind, diesel generators, batteries, and load demand. The test system being examined was an IEEE-15 bus system, in which the beta and Weibull distributions were employed to model the uncertain behavior of RES.

A.   Base Case

The voltage fluctuations observed across multiple buses offer valuable insights into the system's stability and operational robustness. Minor

discrepancies in standard voltage levels can trigger equipment with low tolerance to fail or activate its inbuilt safety mechanisms, which in turn may lead to a series of system failures. The voltage profile for the base case is shown in Fig. 9. The data suggests that buses 13 and 15 exhibit the greatest voltage fluctuations in high-stress situations. These buses require regular monitoring and potential upgrades, which may involve installing voltage stabilizers or altering the local power grid's schedules.
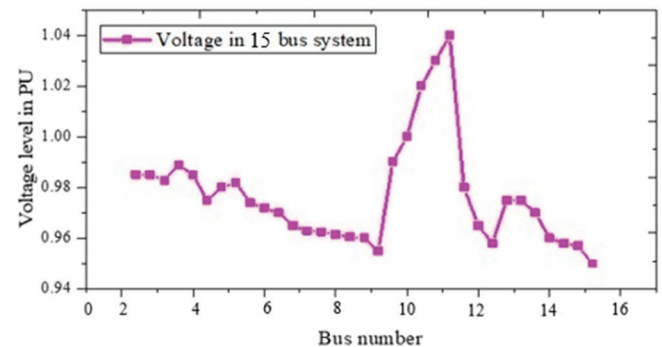

Fig. 9. Voltage profile for base case

B.   Effect of ESS on Voltage Profile

Being a part of isolated microgrids, BESS helps keep energy balance and stable voltage. How much charge each battery has plays a role in governing the operation of PV arrays and wind turbines. When there is a high SoC, MPPT technology lets renewables produce maximal energy and then stores any extra energy. If the SoC is too low, they rearrange operations so the device uses less energy and functions smoothly. The impact of BESS on the voltage profile is depicted in Fig. 10.
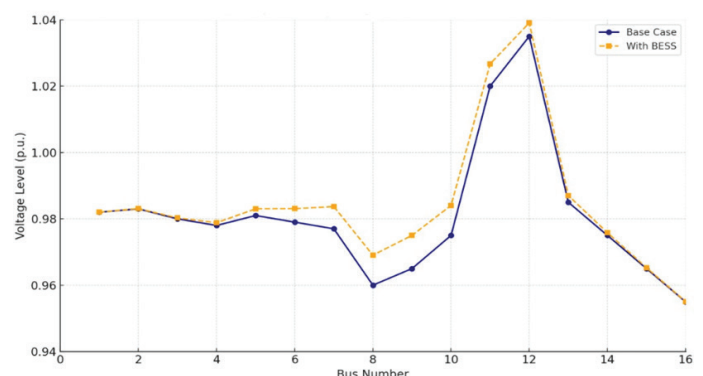

Fig. 10. Impact of BESS on voltage profile

The system's voltage and its general accuracy are best maintained when the amount of energy made by renewable sources is cut down by additional

restrictions. This is possible as they manage their generation according to clear criteria, which allows them to stop sudden swings in voltage and support grid stability. By following this method, the BESS can be recharged precisely, prevent over- or under-charging, and ready more energy for urgent uses and power-off emergencies.

C.   Effect of Load Variation on Voltage Profile

Ensuring that voltage is balanced in isolated microgrids is the main aim of BSPCE which it achieves by placing the right limits on distributed generation and adjusting output to fit demand overall. Without a major grid, it is important to use demand response because it controls how loads work based on prices and preserves steady voltage in the system. The impact of demand response on voltage profile is depicted in Fig. 11.
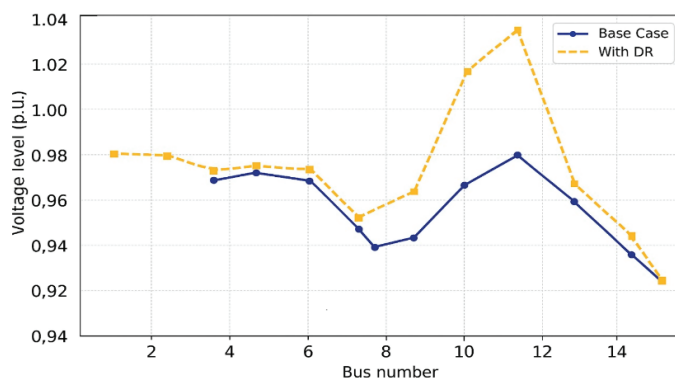
Fig. 11. Impact of load variation on voltage profile

Loads are divided into three groups: those that can be temporarily changed or paused, such as hybrid electric vehicles; those that can be changed but not paused; and those that must always operate, facilitating flexible voltage control and improved system reliability. In Fig. 11, the various strategies are shown affecting voltage profiles throughout the network. Voltage stability is improved by both BESS and demand response, and demand response is highest when looking at bus 11. A small drop in voltage happens when plug-in hybrid electric vehicles (PHEVs) are alternating with other vehicles.

D.   Impact of EV on Voltage Distribution

The increase in electric vehicles is causing new problems with voltage levels in distribution systems. The high power used in peak-time charging can sometimes cause brief drops in voltage, adding stress to the infrastructure and raising the chance of disturbances. Voltage stability needs to be preserved, the grid must be resilient, and electric vehicle charging needs to be smoothly integrated, so it is important to take these impacts into account. Comparative analyses of distributed locational marginal price (DLMP) profiles for multiple bus numbers are illustrated in Fig. 12, demonstrating the effects of various energy management strategies on voltage accuracy. The incorporation of BESS leads to reduced and slightly lower DLMP values, specifically between buses 8 and 10, signifying improved voltage regulation and more balanced power flow. Unlike PHEVs, which generate moderate DLMP increases beyond bus 12 due to increased charging demand, this can also result in localized voltage fluctuations.
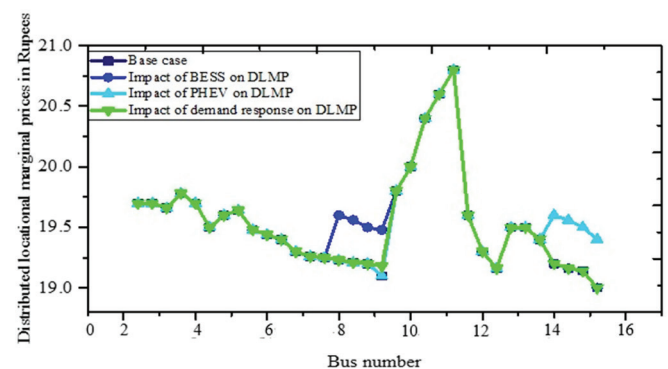
Fig. 12. DLMP profile comparison for all the 4 cases

The demand Response scenario exhibits the most significant DLMP fluctuations, particularly around bus 11, illustrating the dynamic load shifts and their impact on voltage accuracy.

In order to evaluate the accuracy of the surrogate model, we conducted a series of comparative tests, using the surrogate model in comparison to full-scale power system simulations for a set of diverse contingency scenarios. The proposed method, BSPCE, has high accuracy at low cost with a proper account of the complex input distributions and, therefore, is quite appropriate for the practical power system with uncertain renewable sources. The methods of surrogate modeling and uncertainty quantification in power systems are compared in Table I.

TABLE I. COMPARATIVE STUDY OF SURROGATE MODELING AND UNCERTAINTY QUANTIFICATION METHODS IN POWER SYSTEMS

Method	Accuracy	Computational Cost	Complexity	Advantages	Limitations	Suitability for IMG
MCS	High	Very High	Low	Conceptually Simple, Distribution-Free	Poor performance under large workloads	Low
PE	Moderate	Low	Moderate	Rapid Execution, Resource-Efficient	Poor scalability	Moderate
Kriging	High	Moderate-High	High	Accurate Modeling, Interval Estimation	Complex to implement	Moderate
Neural Networks	Variable	High	High	Input Flexibility, Nonlinear Mapping	Lacks transparency	Moderate to low
BSPCE (Proposed)	High	Low	Moderate	Adaptive Accuracy, Sparse Efficiency	Struggle with high-dimensional problems	High

Comparisons of voltage magnitudes and line loadings between the two models are shown in Table II. The mean absolute error (MAE) by the surrogate model was found to be 0.007 p.u. and the mean relative error (MRE) was 0.69%, which is a strong agreement with the detailed simulation results.

TABLE II. VALIDATION OF SURROGATE MODEL RESULTS AGAINST FULL SIMULATIONS

Metric	Full Simulation	Surrogate Output	Rel. Error (%)
Voltage at Bus 13 (p.u.)	0.984	0.977	0.71
Voltage at Bus 15 (p.u.)	0.963	0.956	0.73
Frequency Deviation (Hz)	0.021	0.022	4.76
Line Loading (%)	73.1	71.8	1.78

Further, the surrogate model proved successful for real time power system analysis for screening and decision making in the sense that, on average the computation time has been reduced by about 92%.

V. CONCLUSION

This study introduces an Adaptive Bayesian Sparse Polynomial Chaos Expansion framework to tackle the difficulties of voltage control in isolated microgrids under conditions of uncertainty. The proposed adaptive method adjusts sampling dynamically according to a model's sensitivity and approximation error, leading to enhanced computational efficiency and greater accuracy, particularly in areas of heightened uncertainty. When applied to the modified IEEE-15 bus test system, the proposed method successfully measures the uncertainties related to maximum load capacity, the variability of renewable energy, and operational restrictions, simultaneously incorporating the functions of battery energy storage systems, electric vehicles, and demand response systems. The results show that the proposed framework effectively captures intricate input relationships and patterns and accurately represents voltage behavior during high-demand situations. Buses 13 and 15 showed the most significant voltage instability, highlighting the necessity for concentrated improvements. The strategic operation of battery energy storage systems and load shifting through demand response have a substantial positive impact on voltage profiles and DLMP stability. The validation of the surrogate model against full-scale simulations revealed a high degree of accuracy, with an MAE of 0.007 p.u. and an MRE of 0.69%. This adaptive BSPCE-based approach offers a reliable tool for boosting voltage stability, streamlining energy management, and increasing the operational resilience of isolated microgrids under conditions of high uncertainty.

References

[1] Z. Shuai, W. Huang, X. Shen, Y. Li, X. Zhang, and Z. J. Shen, "A Maximum Power Loading Factor (MPLF) Control Strategy for Distributed Secondary Frequency Regulation of Islanded Microgrid," *IEEE Trans Power Electron*, vol. 34, no. 3, pp. 2275–2291, Mar. 2019, doi: 10.1109/TPEL.2018.2837125.

[2] P. Yang, C. Zheng, Z. Xu, T. He, X. Yin, and S. Shen, "Power coordinated control of the islanded multi-layer microgrids," in *2016 IEEE Innovative Smart Grid Technologies - Asia (ISGT-Asia)*, IEEE, Nov. 2016, pp. 1145–1150. doi: 10.1109/ISGT-Asia.2016.7796547.

[3] J. A. da Silva Neto, E. V. N. de Lorenci, and A. C. Z. de Souza, "Voltage Stability Analysis Using Energy Function Considering the Transmission-Microgrid Coupling and Microgrid Operation in Islanded Mode," in *2020 International Conference on Power, Instrumentation, Control and Computing (PICC)*, IEEE, Dec. 2020, pp. 1–6. doi: 10.1109/PICC51425.2020.9362399.

[4] S. Kumar, I. Ali, and A. S. Siddiqui, "Control of Wind Energy Connected Single Phase Grid with MPPT for Domestic Purposes," in *2022 2nd International Conference on Intelligent Technologies (CONIT)*, IEEE, Jun. 2022, pp. 1–6. doi: 10.1109/CONIT55038.2022.9847854.

[5] D. Jiang, M. Yu, and Z. Dou, "Maximum power point tracking (MPPT) techniques in distributed photovoltaic generation systems," in *Fourth International Conference on Testing Technology and Automation Engineering (TTAE 2024)*, S. S. Aphale and A. Jha, Eds., SPIE, Dec. 2024, p. 133. doi: 10.1117/12.3055616.

[6] Muthuvel Raj Suyambu and Pawan Kumar Vishwakarma, "Improving grid reliability with grid-scale Battery Energy Storage Systems (BESS)," *International Journal of Science and Research Archive*, vol. 13, no. 1, pp. 776–789, Sep. 2024, doi: 10.30574/ijsra.2024.13.1.1694.

[7] M. Minetti, G. B. Denegri, and A. Rosini, "New Approaches to Reactive Power Sharing and Voltage Control in Islanded AC Microgrids," in *2020 55th International Universities Power Engineering Conference (UPEC)*, IEEE, Sep. 2020, pp. 1–6. doi: 10.1109/UPEC49904.2020.9209864.

[8] H. Chappa and T. Thakur, "A novel load shedding methodology to mitigate voltage instability in power system," *Electrical Engineering & Electromechanics*, no. 3, pp. 63–70, May 2022, doi: 10.20998/2074-272X.2022.3.09.

[9] D. Fehrle, C. Heiberger, and J. Huber, "Polynomial Chaos Expansion: Efficient Evaluation and Estimation of Computational Models," *Comput Econ*, vol. 65, no. 2, pp. 1083–1146, Feb. 2025, doi: 10.1007/s10614-024-10772-5.

[10] J. Liu, Y. Shi, C. Ding, and M. Beer, "Efficient global sensitivity analysis framework and approach for structures with hybrid uncertainties," *Comput Methods Appl Mech Eng*, vol. 436, p. 117726, Mar. 2025, doi: 10.1016/j.cma.2024.117726.

[11] A. A. Eajal, A. H. Yazdavar, E. F. El-Saadany, and K. Ponnambalam, "On the Loadability and Voltage Stability of Islanded AC–DC Hybrid Microgrids During Contingencies," *IEEE Syst J*, vol. 13, no. 4, pp. 4248–4259, Dec. 2019, doi: 10.1109/JSYST.2019.2910734.

[12] J. Kweon, H. Jing, Y. Li, and V. Monga, "Small-signal stability enhancement of islanded microgrids via domain-enriched optimization," *Appl Energy*, vol. 353, p. 122172, Jan. 2024, doi: 10.1016/j.apenergy.2023.122172.

[13] M. H. Hemmatpour, "Optimum Interconnected Islanded Microgrids Operation with High Levels of Renewable Energy," *Smart Science*, vol. 7, no. 1, pp. 47–58, Jan. 2019, doi: 10.1080/23080477.2018.1540379.

[14] X. Xu *et al.*, "Maximum Loadability of Islanded Microgrids With Renewable Energy Generation," *IEEE Trans Smart Grid*, vol. 10, no. 5, pp. 4696–4705, Sep. 2019, doi: 10.1109/TSG.2018.2848958.

[15] M. M. Aman, G. B. Jasmon, A. H. A. Bakar, and H. Mokhlis, "Optimum network reconfiguration based on maximization of system loadability using continuation power flow theorem," *International Journal of Electrical Power & Energy Systems*, vol. 54, pp. 123–133, Jan. 2014, doi: 10.1016/j.ijepes.2013.06.026.

[16] W. T. El-Sayed, H. E. Z. Farag, H. H. Zeineldin, and E. F. El-Saadany, "Formation of Islanded Droop-Based Microgrids With Optimum Loadability," *IEEE Transactions on Power Systems*, vol. 37, no. 2, pp. 1564–1576, Mar. 2022, doi: 10.1109/TPWRS.2021.3099691.

[17] Z. Lu, X. Xu, Z. Yan, and H. Wang, "Density-based Global Sensitivity Analysis of Islanded Microgrid Loadability Considering Distributed Energy Resource Integration," *Journal of Modern Power Systems and Clean Energy*, vol. 8, no. 1, pp. 94–101, 2020, doi: 10.35833/MPCE.2018.000580.

[18] K. He, X. Xu, H. Wang, and Z. Yan, "Global Sensitivity Analysis of Islanded Microgrid Power Flow," in *2018 IEEE Power & Energy Society General Meeting (PESGM)*, IEEE, Aug. 2018, pp. 1–5. doi: 10.1109/PESGM.2018.8586617.

[19] J. C. García-Merino, C. Calvo-Jurado, and E. García-Macías, "Sparse polynomial chaos expansion for universal stochastic kriging," *J Comput Appl Math*, vol. 444, p. 115794, Jul. 2024, doi: 10.1016/j.cam.2024.115794.

[20] J. Devi, G. Kotalczyk, and F. E. Kruis, "Accuracy control in Monte Carlo simulations of particle breakage," *Int J Model Identif Control*, vol. 31, no. 3, p. 278, 2019, doi: 10.1504/IJMIC.2019.098774.

[21] E. Pchelintsev, S. Pergamenshchikov, and M. Povzun, "Efficient estimation methods for non-Gaussian regression models in continuous time," *Ann Inst Stat Math*, vol. 74, no. 1, pp. 113–142, Feb. 2022, doi: 10.1007/s10463-021-00790-7.

[22] J. Grote and C. Thäle, "Gaussian polytopes: A cumulant-based approach," *J Complex*, vol. 47, pp. 1–41, Aug. 2018, doi: 10.1016/j.jco.2018.03.001.

[23] A. A. Eajal, A. H. Yazdavar, E. F. El-Saadany, and K. Ponnambalam, "On the Loadability and Voltage Stability of Islanded AC–DC Hybrid Microgrids During Contingencies," *IEEE Syst J*, vol. 13, no. 4, pp. 4248–4259, Dec. 2019, doi: 10.1109/JSYST.2019.2910734.

[24] Z. Wang and J. Yang, "Distributed Secondary Control Strategy with Dynamic Event Triggering for Islanded Microgrids," in *2024 Second International Conference on Cyber-Energy Systems and Intelligent Energy (ICCSIE)*, IEEE, May 2024, pp. 1–6. doi: 10.1109/ICCSIE61360.2024.10698572.

[25] M. M. A. Abdelaziz and E. F. El-Saadany, "Maximum loadability consideration in droop-controlled islanded microgrids optimal power flow," *Electric Power Systems Research*, vol. 106, pp. 168–179, Jan. 2014, doi: 10.1016/j.epsr.2013.08.020.

[26] M. Thapa, S. B. Mulani, A. Paudel, S. Gupta, and R. W. Walters, "Adaptive Sparse Polynomial Chaos Expansion based on a Classifier with Sequential Sampling," in *AIAA SCITECH 2023 Forum*, Reston, Virginia: American Institute of Aeronautics and Astronautics, Jan. 2023. doi: 10.2514/6.2023-0740.

[27] S. Kumar, I. Ali, and A. S. Siddiqui, "Energy management in a grid-connected microgrid using hybrid Golden Jackal optimization and gradient descent optimization and the concept of loadability," *e-Prime - Advances in Electrical Engineering, Electronics and Energy*, vol. 9, p. 100763, Sep. 2024, doi: 10.1016/j.prime.2024.100763.

[28] S. E. Eyimaya and N. Altin, "Review of Energy Management Systems in Microgrids," *Applied Sciences*, vol. 14, no. 3, p. 1249, Feb. 2024, doi: 10.3390/app14031249.

[29] G. Lai, D. Wang, Z. Wang, F. Fan, Q. Wang, and R. Wang, "Distribution-based PV module degradation model," *Energy Sci Eng*, vol. 11, no. 3, pp. 1219–1228, Mar. 2023, doi: 10.1002/ese3.1401.

[30] Q. Salem, R. Aljarrah, M. Karimi, and A. Al-Quraan, "Grid-Forming Inverter Control for Power Sharing in Microgrids Based on P/f and Q/V Droop Characteristics," *Sustainability*, vol. 15, no. 15, p. 11712, Jul. 2023, doi: 10.3390/su151511712.

[31] S. Yadav, P. Kumar, and A. Kumar, "Grey wolf optimization based optimal isolated microgrid with battery and pumped hydro as double storage to limit excess energy," *J Energy Storage*, vol. 74, p. 109440, Dec. 2023, doi: 10.1016/j.est.2023.109440.

[32] Z. Yao and J. Gan, "Review of Charging and Discharging Strategies for EVs Based on DR," in *2023 25th European Conference on Power Electronics and Applications (EPE'23 ECCE Europe)*, IEEE, Sep. 2023, p. P.1-P.8. doi: 10.23919/EPE23ECCEEurope58414.2023.10264664.

[33] O. T. Adenuga and S. Krishnamurthy, "An MINLP Optimization Method to Solve the RES-Hybrid System Economic Dispatch of an Electric Vehicle Charging Station," *World Electric Vehicle Journal*, vol. 16, no. 5, p. 266, May 2025, doi: 10.3390/wevj16050266.